PNAS

RESEARCH ARTICLE | ENGINEERING

Shear transformations in metallic glasses without excessive and predefinable defects

Zhen Zhang[a], Jun Ding[a,1] [ID], and Evan Ma[a,1]

Plastic flow in metallic glasses (MGs) is known to be mediated by shear transformations (STs), which have been hypothesized to preferentially initiate from identifiable local "defect" regions with loose atomic packing. Here we show that the above idea is incorrect, i.e., STs do not arise from signature structural defects that can be recognized *a priori*. This conclusion is reached via a realistic MG model obtained by combining molecular dynamics (MD) and Monte Carlo simulations, achieving liquid solidification at an effective cooling rate as slow as 500 K/s to approach that typical in experiments for producing bulk MGs. At shear stresses before global yielding, only about 2% of the total atoms participate in STs, each event involving typically ~10 atoms. These observations rectify the excessive content of "liquid-like regions" retained from unrealistically fast quench in MD-produced glass models. Our findings also shed light on the indeterministic aspect of the ST sites/zones, which emerge with varying spatial locations and distribution depending on specific mechanical loading conditions.

metallic glass | shear transformations | Monte Carlo | molecular dynamics simulation

Metallic glasses (MGs) are not only of practical interest due to their unusual mechanical properties (1–11), but also invaluable model systems for understanding the behavior of amorphous solids (6, 12, 13). Generally speaking, a MG is expected to possess intrinsic heterogeneities in both its dynamics and internal local structure, which respond inhomogeneously to external stimuli such as a temperature rise and mechanical loading (14). The basic event underlying the deformation of MGs involves the ST largely confined in a shear transformation zone (STZ) (1–3); the nature of STs has been extensively investigated over the past decades (2, 15–23). The generally accepted picture depicts STZ as a local group of around 100 atoms (or about 1.5 nm in diameter) collectively rearranging under externally applied stresses, and these STZs are closely related to the liquid-like regions retained in the MG structure (6, 24). This common belief, however, is based on phenomenological models (e.g., ref. (16)) and atomistic simulations (e.g., ref. 17) and difficult to verify via direct experimental observations.

In particular, atomistic (e.g., molecular dynamics, MD) simulations carried out thus far in the MG field invariably suffer from the limitation that unrealistically high cooling rates had to be used (usually larger than 10^9 K/s), leading to a long-standing concern that the computer-generated MGs would be very different from the experimental ones from liquid solidification (25–30). For example, the shear modulus of any MD-simulated glass has always been far below that of the corresponding MG made in the laboratory. It is therefore obvious that the mechanisms derived from the MD simulations would not be entirely germane to real-world BMGs. To address this issue, efforts have been continuously made to bridge the gap between the quench rates in simulations versus those in experiments. Berthier and co-workers have done a series of work in this direction, by using the swap Monte Carlo (MC) algorithm (31) to produce highly stable configurations even down to the experimental glass transition temperature (32–34). It was recently shown for two modified Lennard–Jones mixtures (35) that as the effective cooling rate is lowered, thermodynamic properties such as configurational entropy can be measured down to experimental T_g, and a qualitative change in the mechanical behavior of the glass (i.e., with increasing brittleness) can be observed (34). However, a clear picture of the structural and mechanical inhomogeneities has remained elusive, especially when it comes to the characteristic features of the elementary plasticity carriers (i.e., STZs) and their behavior upon yielding of the MG.

Along this line of thought, we begin with the following thought experiment: The structure of BMGs would be expected to become increasingly homogeneous (everywhere) with decreasing cooling rate of the parent liquid and/or extended relaxation/aging below the glass transition temperature, eventually diminishing almost all "liquid-like regions" conducive to STs. As a result, the STZs responding to external stresses/loading would become far less populous than previously observed in the MD simulations and very small

Significance

In conventional metals, the plasticity is mediated by well-defined dislocations and point defects. In contrast, the elementary plasticity carriers in MGs have remained poorly understood thus far, due on the one hand, to the lack of direct experimental observations, and on the other hand, to the limitations of prior phenomenological theories/simulations. Here, by using a highly efficient numerical method we have produced a computer model of $Cu_{50}Zr_{50}$ MG with an effective cooling rate approaching that typical of experimental bulk MGs. This realistic model reveals that shear transformation zones are considerably fewer and smaller than previously believed and cannot be attributed to clear-cut local defects that can be pre-defined in the glass structure.

Author affiliations: [a]Center for Alloy Innovation and Design (CAID), State Key Laboratory for Mechanical Behavior of Materials, Xi'an Jiaotong University, Xi'an, 710049, China

in size toward the ~10 atoms known to be needed to trigger the STs (22, 36), with little chance to cascade into the surrounding neighborhood. However, it has not been possible so far, experimentally or in simulations, to explore the scenario envisioned above. We can now reach this intrinsic limit, via modeling the MG using an approach combining MD and MC simulations. Through this method, we cool the $Cu_{50}Zr_{50}$ liquid at an effective cooling rate as slow as 500 K/s to approach that typical in experiments for producing BMGs, aiming to produce new insight unreachable from the ultrafast quench used in all previous MD simulations.

The embedded atom method (EAM) potentials by Mendelev et al. (37) were used for describing the interatomic interactions. A typical melt-quench procedure under zero pressure was adopted for the MD-only simulations (cooling rate $\geq 10^9$ K/s). The hybrid MD/MC scheme adds a MC cycle at the end of every ten MD steps, allowing for the swaps of local atoms during the MC steps, while the MD integration steps account for the relaxations. As such, the standard MD dynamics were supplemented with structural relaxation to an unprecedented level. Simulations were carried out in the variance constrained semi-grand canonical (VC-SGC) ensemble (38). More details about the parameter setting, e.g., temperature profile and MD/MC integration, are given in the *Materials and Methods*.

Results

MGs Prepared using Various Effective Cooling Rates. To begin with, we present in Fig. 1A the cooling curves, i.e., per-atom potential energy as a function of temperature. One recognizes that the coupling of MD and MC can significantly lower the energy state of the resulting glass relative to the MD-only method (note that the total simulation time increases from MD/MC-1 to MD/MC-4.). In addition, a glass transition (i.e., the deflection of the curve at intermediate temperatures) is seen in all cases, indicating that the MD/MC method indeed mimics the melt-quench procedure as it is usually adopted in conventional MD for producing model glasses, but with a much higher efficiency in accelerating the structural relaxation. Next, we estimate the effective cooling rates achievable using the hybrid MD/MC method through extrapolating the cooling rate dependence of the potential energy of the MD-simulated $Cu_{50}Zr_{50}$ glass at 300 K. Fig. 1B shows that a logarithmic fit describes very well the cooling rate dependence of the MD-simulated $Cu_{50}Zr_{50}$ glass at 300 K (red-filled circles).

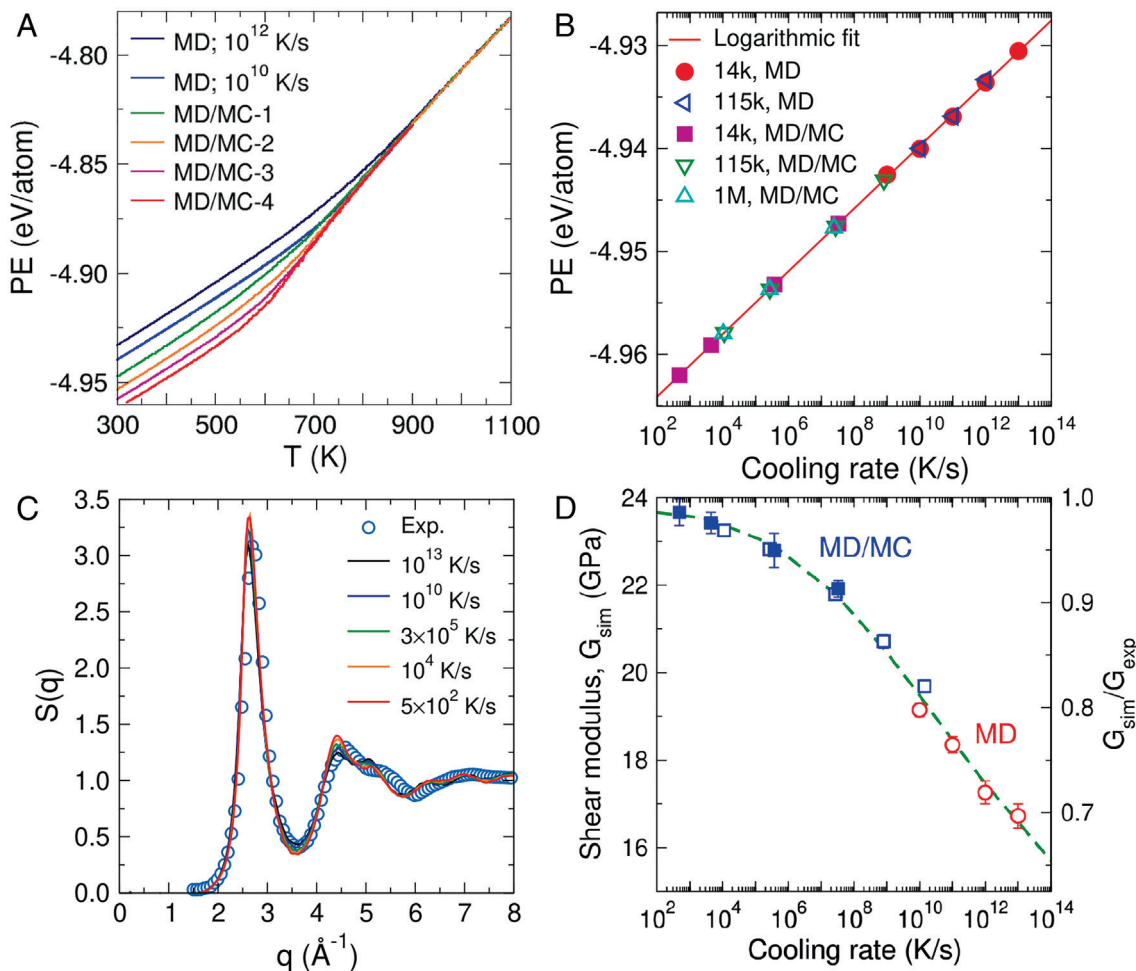**Fig. 1.** $Cu_{50}Zr_{50}$ MG models prepared using various effective cooling rates. (A) Variation in per-atom potential energy (PE) with temperature for the $Cu_{50}Zr_{50}$ MGs prepared using different effective cooling rates. (B) The per-atom potential energy estimated at 300 K vs. effective cooling rate. 14 k, 115 k, and 1 M represent, respectively, samples containing 14,000, 115,000, and 1,000,000 atoms. The solid line is a logarithmic fit to the MD data of the 14 k samples. Error bars are smaller than the symbol size. (C) Total weighted X-ray structure factor, $S(q)$, at a variety of effective cooling rate. The experimental total X-ray structure factor for the $Cu_{50}Zr_{50}$ MG, from ref. 40, is also included for comparison. (D) Simulated shear modulus G_{sim} vs. effective cooling rate. Open and solid symbols are for the 14 k and 115 k samples, respectively. The dashed line is a guide to the eye. To calculate the ratio (see the right ordinate) between the simulated and experimental G, the latter is taken to be 24 GPa, measured from the stress–strain response of a $Cu_{50}Zr_{50}$ MG from ref. 41.

Extrapolation of this trend to lower cooling rates indicates that the hybrid MD/MC method has yielded very slow effective cooling rate, down to 5×10^2 K/s for the small MG samples (containing 14,000 atoms), and 10^4 K/s for the largest samples (containing 1,000,000 atoms). This was achieved at a moderate computational cost, demonstrating the high computational efficiency of the applied MD/MC method. It is worth noting that we detected no sign of crystallization in all the simulated samples, through a careful analysis of the local environment of each atom up to the second neighbor shell (39), affirming that all the computer MGs we have obtained are fully amorphous.

This dramatically reduced effective cooling rate, toward a level almost equivalent to that under laboratory experimental conditions for producing BMGs, yields glass models that are more realistic in terms of their macroscopic properties. Fig. 1C shows their total X-ray structure factor, $S(q)$, of simulated $Cu_{50}Zr_{50}$ MGs with different cooling rates. One notices that the agreement between the simulated and the experimental $S(q)$ (40) becomes progressively better, notably the first and the second peak, with decreasing cooling rates. Furthermore, Fig. 1D shows that the shear modulus G of the simulated MG continuously increases with lowering cooling rate. Previously, all the MD-simulated MGs are at least 20% smaller in G compared with experimental data, due primarily to the unrealistically high cooling rates (see, e.g., ref. 10). Remarkably, this 20% deficiency of G is gradually rectified in the MD/MC-simulated glasses as the effective cooling rate is lowered to the level comparable to that typical in experiments. Note that we are not shooting for a precise value of G, since on the one hand the G estimated from simulations could be interatomic potential-dependent, and on the other hand, the experimental value of G ranges from 24 to 31 GPa, depending on the geometry of the tested specimen and the technique used for the measurement 41,42.

In *SI Appendix*, Fig. S1, we provide additional results illustrating the glass transition temperature, fraction of Cu-centered full icosahedra, boson peak, uniaxial tensile strength, shear localization

behavior, and radial distribution function. All of these properties exhibit a smooth cooling rate dependence over 10 decades, indicating that the MD/MC method can not only produce MG models that are highly consistent with the MD-simulated ones, but also enable the coverage down to processing conditions on par with those in laboratory experiments.

Evolution of Structural Inhomogeneity. The influence of cooling rate is also obvious at the microscopic scale, in terms of the distribution of various atomic-level properties that can serve as indicators of the local structural environment and reflect the inhomogeneity of the latter. In Fig. 2, we show two representative local properties at 300 K, namely the vibrational displacement, λ (*Top* panels), which reflects the local configurational constraints, and the thermal activation energy, E_{act} (*Bottom* panels), as a metric for the ease of thermally activated relaxation (simulation details are given in the *Materials and Methods*), for three MG samples prepared with an effective cooling rate of 10^{13} K/s (hyperquenched, via MD), 10^9 K/s (intermediate, via MD), and 5×10^2 K/s (slowly cooled, via MD/MC).

First, we note that these two local properties correlate quite well with each other, i.e., regions with larger λ tend to have smaller E_{act}, in agreement with the finding of previous simulation studies (43). Importantly, with decreasing cooling rate the distribution of λ and E_{act} becomes progressively less inhomogeneous (i.e., the distribution profile becomes narrower). We find that the relative scales of the inhomogeneities (i.e., the standard deviation divided by the mean of a given property) decrease, from the hyperquenched glass to the slowest-cooled glass, by a factor of two and five for for λ and E_{act}, respectively, indicating that the latter is more sensitive to the change of thermal history for producing the glass. λ shifts toward smaller values, while E_{act} becomes larger, indicating that the glass structure becomes more rigid and less prone to structural relaxation. This finding is consistent with the annealing-induced homogenization of MG as revealed in experiments (44). It is also interesting to note that the distribution profiles are
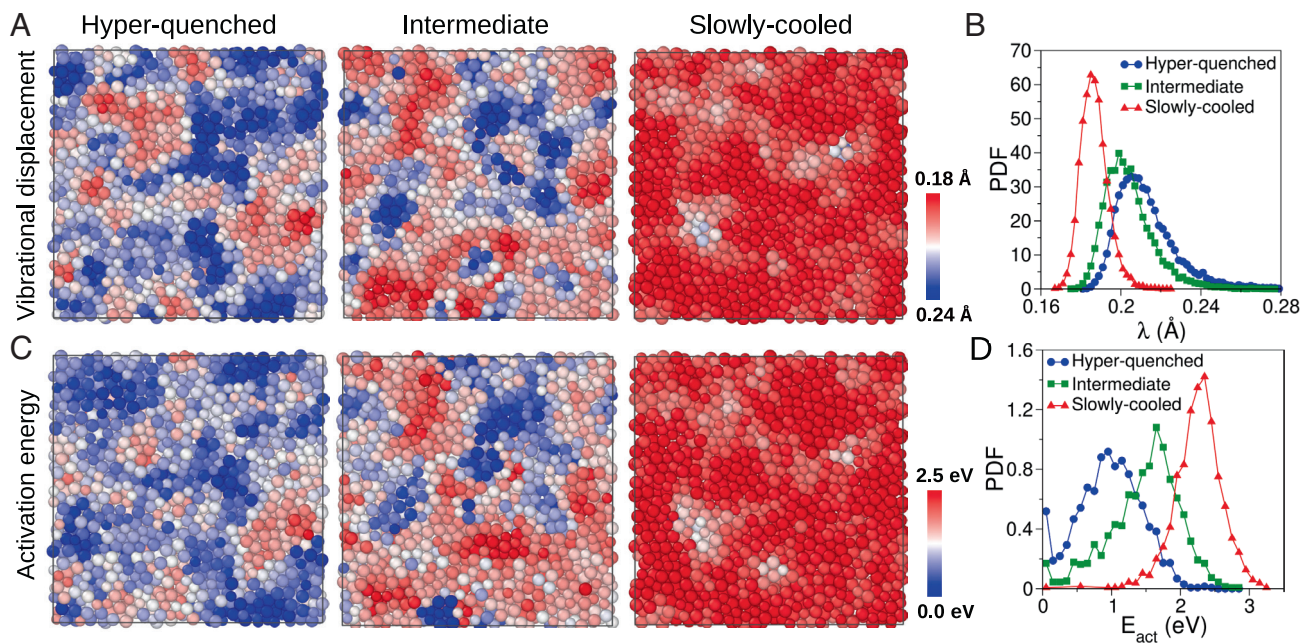

Fig. 2. Inhomogeneity in the MG samples. (A) Snapshots of the MG samples prepared via different effective cooling rates, mapping out the spatial distribution of vibrational displacement, λ.(B) The probability density function (PDF) of λ. (C) The spatial distribution of thermal activation energy, E_{act}. (D) The PDF of E_{act}. For the snapshots, the effective cooling rates are 10^{13} K/s, 10^9 K/s, and 5×10^2 K/s, from left to right, respectively. The samples contain around 14,000 atoms, corresponding to cubes of side length ~6.5 nm at room temperature.

clearly asymmetric, although the characteristic tail becomes less and less prominent with decreasing cooling rate, a result that implies a decreasing concentration of soft spots (45) in the MG.

The homogenization of the local properties promoted via slow cooling is expected to have direct consequences on the stability of the glass (46), as well as the deformation behavior of the MGs. As the glass structure becomes less and less inhomogeneous with the slowing down of cooling the parent liquid, the majority of liquid-like regions (the blue regions in the snapshots, Fig. 2 *A* and *C*) have been relaxed away. As a result, the leftover white-to-blue regions in the snapshots (Fig. 2) appear to have become scarce when compared with the MD-only cases and very small in size, mostly less than ten atoms.

Intrinsic STs in Cu$_{50}$Zr$_{50}$ MGs. To explore the intrinsic deformation events in these well-relaxed glasses, we have performed AQS shear simulations at a step size of 10^{-5} under conserved volume (47) (simulation details are given in the *Materials and Methods*). We have found that this step size is small enough to ensure the convergence of the stress–strain curve and the statistics of the atoms involved in ST events. To begin with, we compare in Fig. 3*A* the stress–strain curves of three representative MGs (same as those in Fig. 2). One observes that, with decreasing cooling rate, the glass becomes increasingly stiffer, reflected by the increasingly steeper slope of the initial portion of the stress–strain curve. Importantly, with decreasing cooling rate the stress drops on

the curve, which are related to ST events, i.e., the elementary carriers of plasticity in MGs (3), become less in number and less pronounced in magnitude; see Fig. 3*B*. An example of such a ST event involving 9 atoms is depicted in the inset of Fig. 3*A*.

Next, we use non-affine squared displacement, D^2_{min} (3), calculated using the atomic configurations immediately before and after a stress drop, as an indicator to identify the atoms that have participated in ST events. We have chosen the threshold value of D^2_{min}, $D_c = 0.18$ Å^2, based on the fact that larger than this value the statistics of STZs does not change in a significant manner and that up to this value the size ratio between the STZs in the slowly quenched glass and the fast-quenched glasses is independent of D_c (see *SI Appendix*, Fig. S2). A recent numerical study has reported that a single stress drop can correspond to multiple STZs (48). We have carefully probed the spatial distribution of ST atoms in our samples and found that the percentage of these multiple STZ-involved stress drops decreases from ~34% for the hyper-quenched glass to ~8% for the slowly cooled glass.

Fig. 3*C* plots the distribution of the STZ sizes, which can be well described by a log-normal function (solid lines). Note that this distribution depends only weakly on the threshold strains over which we count the STZs, *SI Appendix*, Fig. S3. A significant reduction of both the number and the size of the STZs is apparent with decreasing cooling rate. For the hyper-quenched and the intermediate samples, the distribution of N_{STZ} has a pronounced tail toward larger sizes. By contrast, for the slowly cooled sample, not
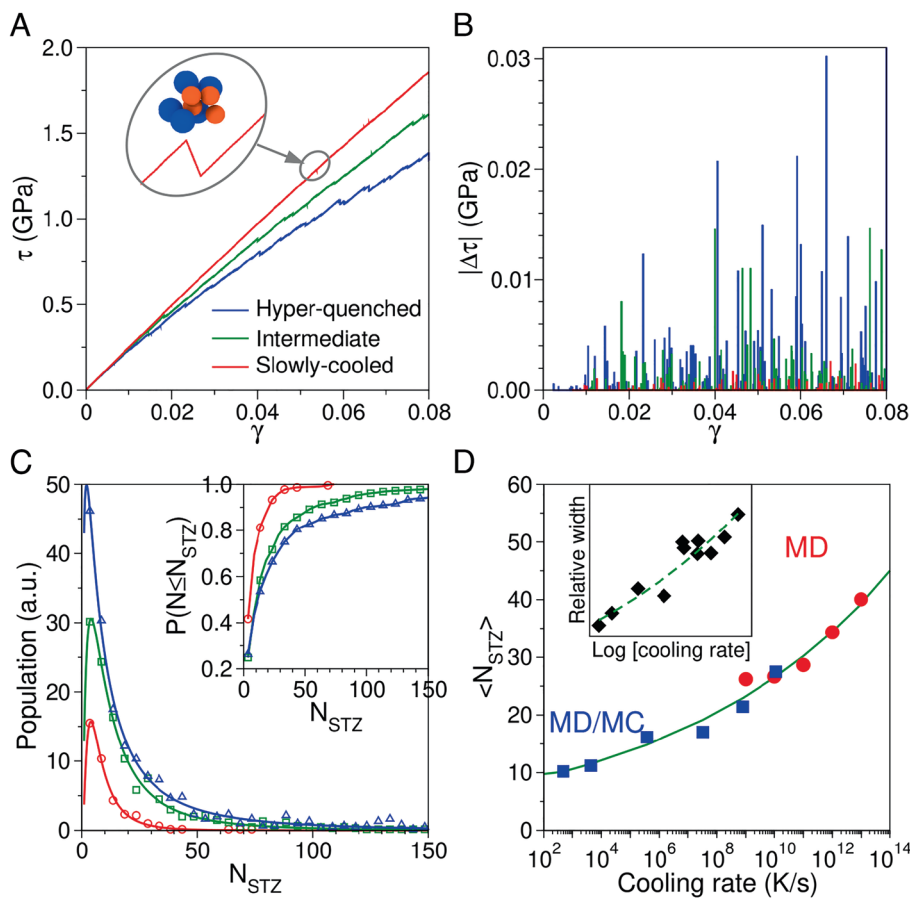

Fig. 3. Shear transformation zones in the MG samples. (*A*) Shear stress (τ)–shear strain (γ) curves for the athermal quasi-static shear of the MG samples in the *xy* direction. The inset is the enlarged view of the stress drop at $\gamma_{xy} = 0.05717$ which is induced by the shear transformation of a cluster of nine atoms (Cu and Zr are represented by balls in orange and blue, respectively). (*B*) The magnitude of stress drops, $|\Delta\sigma|$. (*C*) Distribution of the STZ size. Solid lines are log-normal fits to the data points. The inset shows the cumulative probability $P(N \leq N_{STZ})$, i.e., the probability that the STZ size is smaller than or equal to the corresponding value on the x-axis. (*D*) Cooling rate dependence of the mean STZ size. The number of ST events is counted up to $\gamma = 0.08$. The inset shows the relative width of the distribution profiles in panel (*C*). Lines in panel (*D*) are power-law fitting to all the data points.

only is the number of the STZs significantly reduced, but the distribution of N_{STZ} also becomes much narrower. The cumulative probability in the inset of Fig. 3C shows that 80% of the STZs in the slowly cooled MD/MC sample have $N_{STZ} < 15$, whereas for the MD-hyper-quenched sample, a significant fraction of the STZs have $N_{STZ} > 50$. Fig. 3D shows that the mean size of the STZs decreases from ~40 for the hyper-quenched sample to ~10 for the slowly cooled sample and that the decrease of the mean STZ size with cooling rate can be well described by a power law. It is also worth noting that the spread of the STZ size distribution becomes increasingly narrower at lower cooling rate (and so does the relative width of the distribution profiles, see the inset), in accordance with the reduced degree of inhomogeneity in these samples (see Fig. 2).

For the slowly cooled sample, the STZ typically involves ~10 atoms. This is close to the number of atoms found to be needed for triggering thermally activated local rearrangement (also known as β relaxation) (22, 36); the displacement cutoff for determining the trigger atoms was chosen in such a way that it includes all atoms with abnormally large displacement fluctuations; see ref. 22 for details. This finding suggests that in a well-relaxed glass structure, the external stresses (e.g., via shear) would not be able to expand much in scope the trigger events for localized relaxation, in terms of the number of atoms and the size of the region involved. We also note that the STZ size identified here is only about one half of that estimated in previous studies (e.g., ref. 21, through either a statistical analysis of the first pop-in stress during spherical nanoindentation, or the cooperative shearing model of Johnson and Samwer (16)).

Meanwhile, one would expect that these small clusters of atoms constituting the STZs would be spatially well separated from each

other as each of them has a hard time invading into the surrounding neighborhood. In the following, we show that this is indeed the case by analyzing the spatial distribution of the ST atoms. Fig. 4A presents this distribution for the intermediate sample and the slowly cooled sample, respectively, at the shear strain $\gamma = 0.08$. We observe that the ST atoms in the intermediate sample form percolated networks, whereas in the slowly cooled sample these fertile sites only form small clusters and are isolated from one another. Also, the fraction of the ST atoms declines considerably from the intermediate MG to the slowly cooled MG: Fig. 4B shows quantitatively that the fraction of ST atoms decreased from ~35% in the hyper-quenched MG to only ~2% in the slowly cooled MG. Moreover, Fig. 4C shows for the ST atoms the spatial autocorrelation function, $C(r)$, which is defined as $C(r) = \frac{\langle P_{r_0} P_{r_0+r} \rangle - \langle P_{r_0} \rangle^2}{\langle P_{r_0}^2 \rangle - \langle P_{r_0} \rangle^2}$. Here P denotes D^2_{min}, and P_{r_0} and P_{r_0+r} are, respectively, this property for an atom at a reference position r_0 and the value of the atom at a distance of r from the reference point. One recognizes that the $C(r)$ decays in an exponential manner, which allows for fitting the data using the expression $y = A \times \exp(-x/\xi)$, where A and ξ are fitting parameters and the latter is the decay length. From the hyper-quenched sample to the slowly cooled sample, the decay length ξ is reduced from 3.0 Å to 1.8 Å.

Taken together, these results indicate that all previous MD-simulated MG models have overestimated the fraction of fertile sites for STs and their percolation, inevitably making the glass models more ductile in deformation than real-world MGs. This conclusion is further supported by the deformation behavior of the MGs under uniaxial tension, which shows a gradual transition of the yielding from more ductile (spread-out of STs and
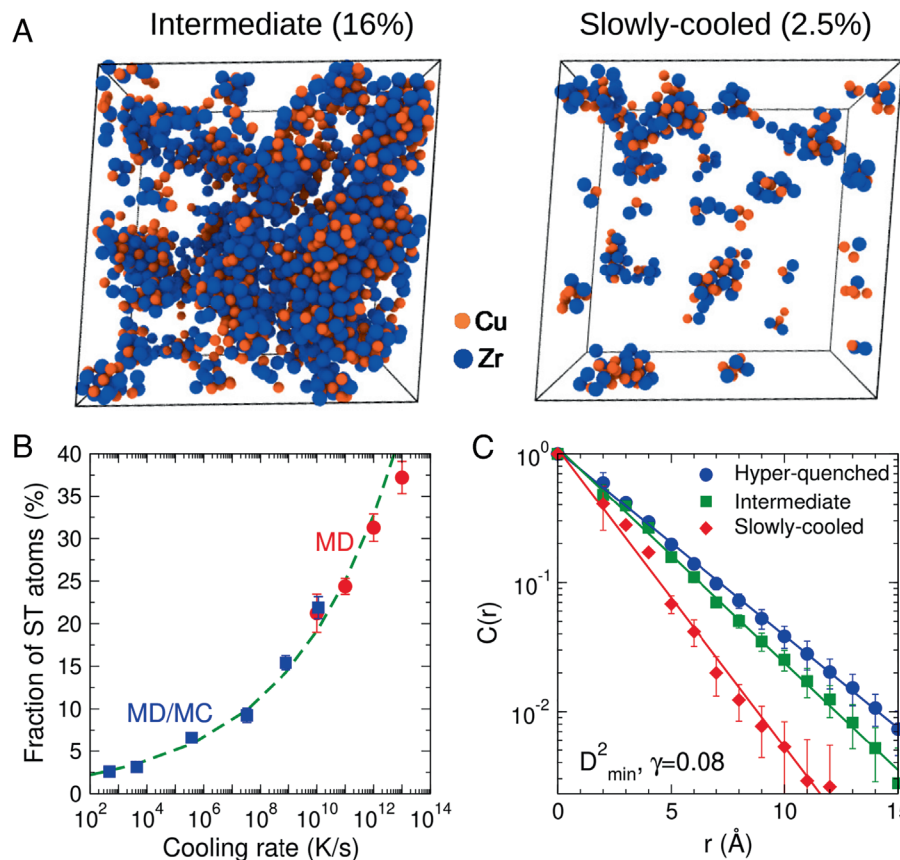

Fig. 4. Shear transformed atoms in the MG samples. (A) Snapshots showing the spatial distribution of the ST atoms at the shear strain $\gamma = 0.08$. The number in the bracket indicates their fraction. (B) Cooling rate dependence of the fraction of the ST atoms. Dashed line is a power-law fit to all the data points. (C) Spatial autocorrelation function of D^2_{min}. Only the ST atoms are considered. Solid lines are exponential fits to the data points.

shear bands, similar to previous MD simulations) to more brittle (higher propensity for strain localization and fewer shear bands) behavior with decreasing cooling rate (see *SI Appendix*, Fig. S4), reminiscent of the effect of extended annealing of the initial sample (49).

Local Structures for the ST-Fertile Sites Inside the Slowly Cooled MG. Having produced MG models that are closer to experiments in terms of their macroscopic properties, a further important question to address is whether the pivotal sites for STs (i.e., ST atoms) have distinct structure and properties such that they can be identified in the as-prepared static structure even before deformation. To shed light on this issue, we decompose the representative parameters of atomic properties that characterize the local structure of the slowly cooled MG sample into contributions from the ST atoms and the rest.

Fig. 5A shows that in terms of the distribution of vibrational displacement λ, the ST atoms exhibit notable difference from the rest sites, in that the distribution for the fertile sites peaks at a considerably larger λ and has a pronounced tail to the right of the distribution. However, the overlap between the two distribution profiles is too strong to allow for a cutoff value that separates apart the two kinds of atomic sites. Fig. 5B shows that the local activation energy E_{act} of the fertile sites is on average smaller than that of the regular sites, but that there is also a strong overlap between the two distributions. Consistent with earlier MD simulation studies on even more heterogeneous MG structures, the sites more

fertile for ST (white regions in Fig. 2) still tend to arise from the quasi-localized soft spots (45) (see plot for ST atoms in Fig. 5A). In other words, the tendency remains that upon loading the STs preferentially arise from high-λ sites than the rest (Fig. 5A). These locations have higher flexibility volume (10) such that the atomic environments are more prone to rearrangements.

Regarding *bona fide* local structural quantities, Fig. 5C shows that the atomic volume for the ST-fertile sites is simply indistinguishable from that for the regular sites. In other words, there are no recognizable (e.g., nanometer sized) "loosely packed regions" relative to (a matrix of) "densely packed regions." Putting it another way, there are no identifiable defects arising from a noticeable deficit in atomic packing density, let alone a Swiss cheese-like density bifurcation (7–9). The atomic coordination number, on the other hand, shows a discernable difference between the two kinds of sites, Fig. 5D, particularly for the Cu atoms: While the most probable coordination number of regular Cu is 12, the fertile Cu atoms are more likely to be found to have a smaller coordination number with the most probable being 11. The observed difference between the coordination number of regular and fertile Cu atoms could be attributed to the high content of the Cu-centered full icosahedra in the glass; see *SI Appendix*, Fig. S1B. Specifically, the regular Cu atoms are in favor of more rigid icosahedral coordination, whereas the ST Cu atoms prefer a local structure that are more disordered. This, on the one hand, results in the smaller coordination number of the fertile Cu atoms relative to that of the regular Cu atoms and, on the other hand, leads to
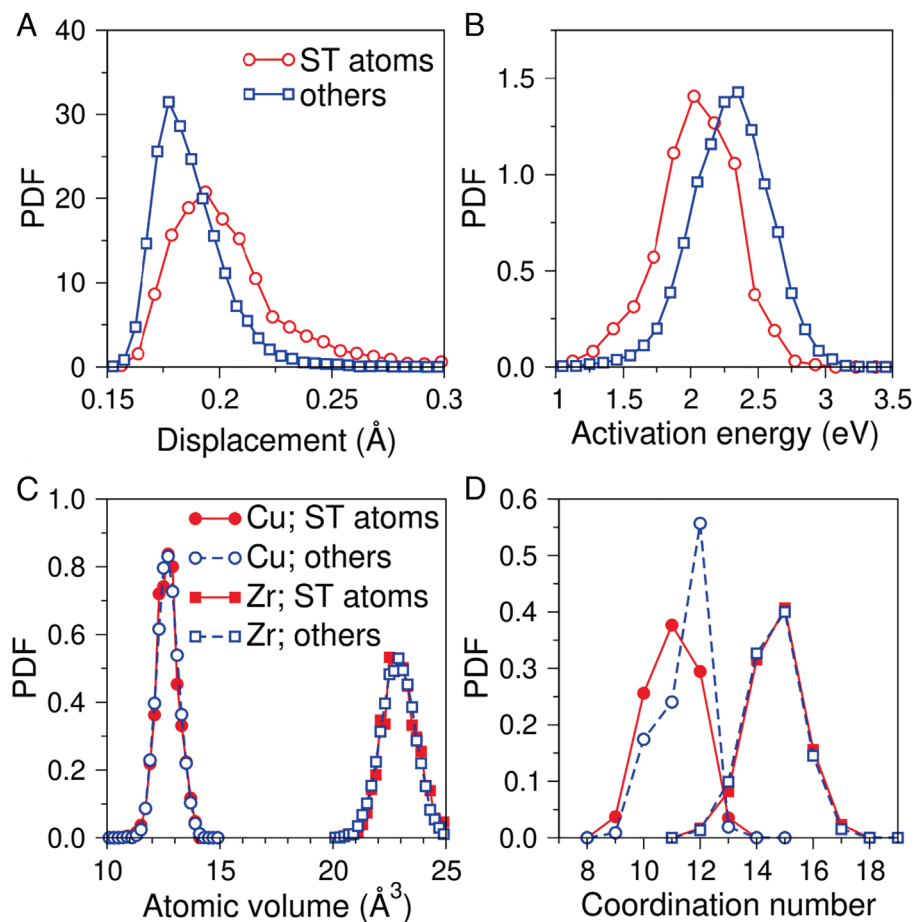

Fig. 5. Behavior of structural indicators in the MG samples. Probability density function (PDF) of (A) the vibrational displacement, (B) local activation energy, (C) atomic (Voronoi) volume, and (D) coordination number. The number ratio between the shear transformed Cu and Zr atoms is around one. These results are for the slowly cooled MG (i.e., via the MD/MC method).

different local chemical order around the two types of atoms; see *SI Appendix*, Table S1. We surmise that the observed difference in the coordination of the two types of atoms may depend on the glass composition, which at occasional MG compositions prefers icosahedral local environments. In *SI Appendix*, Fig. S5, we show that these observations of the insignificant differences between the atomic structures of the two kinds of atomic sites are independent of cooling rate by which the MG sample was prepared.

Discussion

By implementing a hybrid MD/MC method, we have been able to explore the atomic-level properties of the $Cu_{50}Zr_{50}$ MG models produced with effective cooling rates as low as 500 K/s, approaching that typical in experiments for producing bulk MGs. With decreasing cooling rate of the parent liquid, the local structure and properties of the resulting glass become less and less inhomogeneous (for extrinsic factors in liquid solidification that may introduce additional heterogeneity in read-world MG samples, see comments in *SI Appendix*).

The cooling rate dependence of the two main characteristics of STZ, i.e., their mean size and concentration, is found to be well described by a power-law function approaching a saturation plateau. For the slowly cooled MG which is very close to this saturated state, only ~2% of the atoms are found to be fertile sites participating in the STs at the shear stress of ~2 GPa, far less populous than previously believed. The STZs are very small in size, toward the ~10 atoms known to be needed to trigger the thermal activated deformation/relaxation (22). This markedly smaller STZ is due to the increased constraints in the well-relaxed MG for the STZ to expand into its surrounding neighborhood. These findings remove some of the artifacts associated with previous super-fast MD quenching and call into question some existing formulations, with regard to the STZ parameters used in currently prevailing models in the field.

We note that while the MG structure is non-uniform from location to location, the range/spread of inhomogeneity is not as wide as previously believed via MD-alone simulations. Through detailed structural analysis, we have found that the atomic volumes of the sites participating in STs are indistinguishable from those of all the other atoms in the sample. Physics-informed local properties such as atomic vibrational amplitude and thermal activation energy, featuring a tail in their distribution profiles, are more sensitive than purely local structural parameters in revealing the inhomogeneity intrinsic to the MG. Our MD/MC route clearly establishes that intrinsically the MG structure would spontaneously evolve in the direction that eliminates the high-energy "loosely packed regions." Hence, there are no easily recognizable (e.g., from a few angstroms to nanometer in size) defects having markedly lower atomic packing density than the "densely packed regions," let alone an extreme bifurcation into a Swiss cheese-like contrast purported in some papers (7–9). In general, as the local structures are complex and varied, and their (often subtle) differences can influence whether or not atomic rearrangements are provoked in response to a particular loading condition, which also brings in multiple variables/parameters including the loading direction, amplitude, and (often) multiaxial stress state, it is not possible to define atomic flow units that are deterministic for plasticity based on simple parameters of the static local structure inside an as-prepared MG. This is in accordance with an earlier view that STZs are not preexisting defects that can be identified *a priori*, but instead emerge dynamically to respond/couple to applied stresses, producing appreciable atomic rearrangements that accommodate specific imposed strains (21, 22, 50, 51).

Therefore, in order to establish a correlation between the local static glass structure and its rearrangement propensity, a major step forward would have to rely on drastically boosting the amount of information in the local environment, to include multifaceted atomic packing (topological as well as chemical) features as well as influence from their spatial anisotropy. To that end, instead of previously used pair distribution functions (i.e., an average or one-dimensional projection), we could change the input into a huge "matrix" of atomic distribution functions in all directions over the three-dimensional (3D) space. Recent advances in deep learning make it possible to handle such a computationally intensive task (52): A rotationally non-invariant local structure representation, combined with convolutional neural network, achieves a high-fidelity prediction of the loading orientation-dependent plastic susceptibility from static structures in amorphous solids for stress-driven STs.

Conclusions

Exploiting MG models obtained with effective cooling rates as low as those typical in making experimental bulk MGs, we have demonstrated that the spatial extent, population density, and structural characteristics of STs intrinsic to MGs are different from what have been envisaged from some earlier simulations and theories. Only about 2% of the atoms are fertile sites participating in ST events at the stress level typical before yielding, and each event involves on average just ~10 atoms. The idea that deformation relies on loose, low-density regions is unrealistic, but merely a consequence of the excessive fertile sites resulting from artificially high quench rates previously used in MD simulations to obtain the MG structure. ST in MGs is indeterministic in the sense that it is not possible to define atomic flow units that carry plasticity based on any known simple parameter of the static structure. In other words, STZs are not preexisting defects that can be identified *a priori* in the as-prepared MG structure.

Finally, as an outlook, we close with an implication of our conclusions above: Rather than focusing on identifying/delineating in the amorphous structure distinctive "defects" as individual deformation carriers, one should instead seek other avenues (such as an artificial intelligence approach (52)) to establish some degree of predictive ability to link the structural inhomogeneities inherent in the glass with the propensity for local atomic rearrangements (the STZs that dynamically emerge) in response to specific deformation conditions.

Materials and Methods

Simulation of the MGs. Our MD simulations used the EAM potentials optimized recently by Mendelev et al. (37) which is suitable to simulate amorphous Cu-Zr alloys even at relatively low cooling rates. We have produced MG samples of $Cu_{50}Zr_{50}$ via the conventional MD or a hybrid MD/MC method (38).

For the pure MD scheme, a typical melt-quench procedure was adopted for obtaining the glasses with various system sizes. Periodic boundary conditions (PBCs) were applied in all three dimensions. A cubic box containing *N* atoms was first melted at 1,500 K for 0.5 ns to erase the memory of the initial positions of the atoms. Then the temperature was lowered to 1,200 K and kept at this temperature until the sample (in the liquid state) reaches equilibrium, which was confirmed by examining the mean squared displacement (MSD) which showed that the liquid has entered the diffusive region and the mean MSD value is greater than 1,000 Å^2 (corresponding to a simulation duration of ~1.0 ns). The equilibrated liquid sample was then cooled down from 1,200 K to 300 K at various cooling rates (in the range from 10^9 to 10^{13} K/s). For the slowly quenched samples, we have used a two-step cooling protocol to save computation time: The cooling before 900 K was done with $\gamma = 10^{10}$ K/s, and below this temperature the nominal cooling rate was applied. We note that this protocol does not affect the glass transition process as before 900 K,

the liquid is still in equilibrium and its properties are independent of the cooling rate used in this study. After quenching, the glass sample was further relaxed at 300 K for 2.0 ns, which is sufficiently long to ensure the convergence of the glass properties. System sizes range from N = 14,000 to 1,000,000 were considered in our simulations. Five independent melt-quench runs were performed with various cooling rates for the samples consisting of 115,200 atoms. The error bar was estimated as the standard error of the mean of the five runs. The isothermal-isobaric ensemble under zero pressure was used throughout the melt-quench process.

The hybrid MD/MC approach used a novel algorithm described in ref. 38. This hybrid scheme allows for local atom type swaps during the MC steps, whereas the relaxations are accounted for by the MD integration steps. As such, the standard MD dynamics was interrupted at the reward of more efficient structural relaxation. Simulations were carried out in the VC-SGC ensemble with the variance parameter κ chosen to be 1,000. One MC cycle containing N/4 trial moves was initiated every 10 MD steps. The MC temperature which determines the Metropolis acceptance criterion was set to be the same as the MD temperature. We note that the chosen parameters are not necessarily the optimal but instead for illustrating the usefulness of this hybrid scheme for producing highly relaxed MGs.

This hybrid scheme has been efficiently integrated in LAMMPS (53). Our simulations showed that this MD/MC scheme is as efficient as the pure MD scheme in terms of computational cost. However, the former can drive the system into equilibrium using a much smaller number of MD steps at a given temperature relative to the stand-alone MD method. Various nominal cooling rates were adopted depending on the simulated system sizes and the computational time required. In the cases where the melt-quench process was done by the hybrid MD/MC scheme, the as-obtained glass samples were further relaxed using the pure MD scheme at 300 K for 2.0 ns before evaluating the properties of the glasses.

Mechanical Deformation of the MGs. Three types of mechanical deformation were considered in this study, namely volume conserved simple shear, athermal quasi-static shear (AQS) (47), and uniaxial tension. For the simple shear simulations, a strain rate of 5×10^{-5} ps^{-1} was applied for the xy, xz, and yz shearing up to a total shear strain of 0.02. The canonical (NVT) ensemble was used, and 3D PBCs were applied for all simulations. The shear modulus G was calculated by a linear fitting of the stress–strain curve at small strains ($\gamma_{ij} \leq 0.01$, where ij denotes the deforming direction). All simulations were performed at 300 K.

AQS simulations were carried out to probe the occurrence of the ST events during the deformation of the MGs. The samples containing 14,400 atoms were used for the simulations. Simple shears were performed at a step size of 10^{-5}. After each step, the displaced configuration was energy minimized using the conjugate gradient algorithm before imposing further deformation to the sample. We used the non-affine squared displacement, also known as D^2_{min} (3), as an indicator of local STZ. The atoms with a D^2_{min} value (measured using the two configurations immediately before and after a stress drop) greater than 0.18 Å^2 were treated as "shear transformed atoms" (see the main text for discussion regarding the choice of this cutoff threshold).

Uniaxial tension simulations were performed to investigate the formation of shear bands and thus the ductility of the MGs. The glass samples containing 14,400 atoms were replicated 5 and 10 times along the x and y directions, respectively, to produce large samples of dimensions 32 nm × 64 nm × 6.4 nm (x-y-z). These samples were first annealed at 550 K for 0.2 ns and then quenched to 300 K for another 0.1 ns of relaxation. This annealing-relaxation process was performed in the NPT ensemble under zero pressure and with 3D PBCs applied.

We note that this procedure is useful in minimizing the effect of the introduced boundaries from the replication of small samples. Next, the PBC along the x direction was released, and the sample was further relaxed at 300 K for 0.1 ns under the microcanonical (NVE) ensemble. Finally, the samples were subjected to uniaxial tension at the temperature of 300 K along the y direction with a strain rate of 5×10^7 s^{-1}. We have also performed full melt-quench and tensile simulations for a sample of the same dimensions as the replicated ones described above, for the cooling rate of 3×10^7 K/s. No apparent difference in the stress–strain, and shear banding behavior was observed. This justifies that the replication of small sample in our tensile simulations does not result in artifacts in the deformation behavior of the simulated glasses, but rather is an effective operation to reduce the computational cost of generating big glass samples.

All simulations described above were carried out using the Large-scale Atomic/Molecular Massively Parallel Simulator software (LAMMPS) (53). Temperature and pressure were controlled using a Nosé–Hoover thermostat and barostat (54–56). The MD time step was chosen to be 2.0 fs.

Calculation of Atomic-Level Properties. We have evaluated two atomic-level quantities for quantifying the inhomogeneities in the simulated MGs, namely the vibrational displacement, λ, and local activation energy, E_{act}. The vibrational displacement reflects the local configurational constraints and was calculated according to the equation

$$\lambda_i = \sqrt{\langle |\mathbf{r}_i(t) - \mathbf{r}_{i,\text{equil}}|^2 \rangle_{\tau_0}},$$

where $\mathbf{r}_i(t)$ is the position of atom i at time t and $\mathbf{r}_{i,\text{equil}}$ is the equilibrium position of atom i. τ_0 is the time interval over which we take the average. For including enough periods of oscillations, we have chosen τ_0 = 100 ps at 300 K. The vibrational displacement calculated on this timescale contains only the vibrational (i.e., without the diffusional) contribution.

To explore the local potential energy landscape (i.e., the potential energy minima and the saddle points), we have employed the ART nouveau method (22, 36, 57, 58). To study the local excitations of the system, initial perturbations in ART were introduced by applying random displacement on a small group of atoms (an atom and its nearest neighbors). The magnitude of the displacement was fixed, while the direction was randomly chosen. When the curvature of the PEL was found to overcome the chosen threshold, the system was pushed toward the saddle point using the Lanczos algorithm (59). The saddle point is considered to be found when the overall force of the total system is below 0.01 eV Å^{-1}. The corresponding activation energy is thus the difference between the saddle point energy and the initial state energy. For each group of atoms, we employed ~100 ART searches with different random perturbation directions. Since there were at least 10,000 such groups in each of our models, more than one million searches by ART were generated in total. After removing the failed searches and redundant saddle points, ~200,000 different activations, on an average, were identified for each of the samples.

1. F. Spaepen, A microscopic mechanism for steady state inhomogeneous flow in metallic glasses. *Acta Metall.* **25**, 407 (1977).
2. A. S. Argon, Plastic deformation in metallic glasses. *Acta Metall.* **27**, 47 (1979).
3. M. L. Falk, J. S. Langer, Dynamics of viscoplastic deformation in amorphous solids. *Phys. Rev. E* **57**, 7192 (1998).
4. Z. Wang, P. Wen, L. S. Huo, H. Y. Bai, W. H. Wang, Signature of viscous flow units in apparent elastic regime of metallic glasses. *Appl. Phys. Lett.* **101**, 121906 (2012).
5. A. Nicolas, E. E. Ferrero, K. Martens, J.-L. Barrat, Deformation and flow of amorphous solids: Insights from elastoplastic models. *Rev. Mod. Phys.* **90**, 045006 (2018).
6. Y. Q. Cheng, E. Ma, Atomic-level structure and structure–property relationship in metallic glasses. *Prog. Mat. Sci.* **56**, 379 (2011).
7. J. C. Ye, J. Lu, C. T. Liu, Q. Wang, Y. Yang, Atomistic free-volume zones and inelastic deformation of metallic glasses. *Nat. Mat.* **9**, 619 (2010).
8. Q. Wang *et al.*, Unusual fast secondary relaxation in metallic glass. *Nat. Commun.* **6**, 7876 (2015).
9. F. Zhu *et al.*, Correlation between local structure order and spatial heterogeneity in a metallic glass. *Phys. Rev. Lett.* **119**, 215501 (2017).
10. J. Ding *et al.*, Universal structural parameter to quantitatively predict metallic glass properties. *Nat. Commun.* **7**, 13733 (2016).
11. A. L. Greer, Y. Q. Cheng, E. Ma, Shear bands in metallic glasses. *Mat. Sci. Eng. R Rep.* **74**, 71 (2013).
12. T. Egami, D. Srolovitz, Local structural fluctuations in amorphous and liquid metals: A simple theory of the glass transition. *J. Phys. F: Met. Phys.* **12**, 2141 (1982).
13. L. Berthier, G. Biroli, Theoretical perspective on the glass transition and amorphous materials. *Rev. Mod. Phys.* **83**, 587 (2011).
14. G. Jug, A. Loidl, H. Tanaka, On the structural heterogeneity of supercooled liquids and glasses. *Europhys. Lett.* **133**, 56002 (2021).
15. D. Srolovitz, V. Vitek, T. Egami, An atomistic study of deformation of amorphous metals. *Acta Metall.* **31**, 335 (1983).

16. W. L. Johnson, K. Samwer, A universal criterion for plastic yielding of metallic glasses with a $(T/T_g)^{2/3}$ temperature dependence. *Phys. Rev. Lett.* **95**, 195501 (2005).
17. M. Zink, K. Samwer, W. L. Johnson, S. G. Mayr, Plastic deformation of metallic glasses: Size of shear transformation zones from molecular dynamics simulations. *Phys. Rev. B* **73**, 172203 (2006).
18. S. G. Mayr, Activation energy of shear transformation zones: A key for understanding rheology of glasses and liquids. *Phys. Rev. Lett.* **97**, 195501 (2006).
19. D. Pan, A. Inoue, T. Sakurai, M. W. Chen, Experimental characterization of shear transformation zones for plastic flow of bulk metallic glasses. *Proc. Natl. Acad. Sci. U.S.A.* **105**, 14769 (2008).
20. J. D. Ju, D. Jang, A. Nwankpa, M. Atzmon, An atomically quantized hierarchy of shear transformation zones in a metallic glass. *J. Appl. Phys.* **109**, 053522 (2011).
21. I.-C. Choi *et al.*, Estimation of the shear transformation zone size in a bulk metallic glass through statistical analysis of the first pop-in stresses during spherical nanoindentation. *Scr. Mate.* **66**, 923 (2012).
22. Y. Fan, T. Iwashita, T. Egami, How thermally activated deformation starts in metallic glass. *Nat. Commun.* **5**, 5083 (2014).
23. D. Richard, G. Kapteijns, J. A. Giannini, M. L. Manning, E. Lerner, Simple and broadly applicable definition of shear transformation zones. *Phys. Rev. Lett.* **126**, 015501 (2021).
24. J. C. Qiao *et al.*, Structural heterogeneities and mechanical behavior of amorphous alloys. *Prog. Mat. Sci.* **104**, 250 (2019).
25. K. Vollmayr, W. Kob, K. Binder, How do the properties of a glass depend on the cooling rate? A computer simulation study of a lennard-jones system. *J. Chem. Phys.* **105**, 4714 (1996).
26. Y. Liu, H. Bei, C. T. Liu, E. P. George, Cooling-rate induced softening in a Zr50Cu50 bulk metallic glass. *Appl. Phys. Lett.* **90**, 071909 (2007).
27. Y. Zhang *et al.*, Cooling rates dependence of medium-range order development in Cu64.5Zr35.5 metallic glass. *Phys. Rev. B* **91**, 064105 (2015).
28. R. E. Ryltsev, B. A. Klumov, N. M. Chtchelkatchev, K. Yu. Shunyaev, Cooling rate dependence of simulated Cu64.5Zr35.5 metallic glass structure. *J. Chem. Phys.* **145**, 034506 (2016).
29. A. J. E. Bouchbinder, I. Procaccia, Cooling-rate dependence of the shear modulus of amorphous solids. *Phys. Rev. E* **87**, 042310 (2013).
30. M. Fan *et al.*, Effects of cooling rate on particle rearrangement statistics: Rapidly cooled glasses are more ductile and less reversible. *Phys. Rev. E* **95**, 022611 (2017).
31. T. S. Grigera, G. Parisi, Fast Monte Carlo algorithm for supercooled soft spheres. *Physi. Rev. E* **63**, 045102 (2001).
32. L. Berthier, D. Coslovich, A. Ninarello, M. Ozawa, Equilibrium sampling of hard spheres up to the jamming density and beyond. *Phys. Rev. Lett.* **116**, 238002 (2016).
33. A. Ninarello, L. Berthier, D. Coslovich, Models and algorithms for the next generation of glass transition studies. *Phys. Rev. X* **7**, 021039 (2017).
34. A. D. S. Parmar, M. Ozawa, L. Berthier, Ultrastable metallic glasses in silico. *Phys. Rev. Lett.* **125**, 085505 (2020).
35. W. Kob, H. C. Andersen, Testing mode-coupling theory for a supercooled binary lennard-jones mixture I: The van hove correlation function. *Phys. Rev. E* **51**, 4626 (1995).
36. J. Ding *et al.*, Universal nature of the saddle states of structural excitations in metallic glasses. *Mat. Today Phys.* **17**, 100359 (2021).
37. M. I. Mendelev, Y. Sun, F. Zhang, C. Z. Wang, K. M. Ho, Development of a semi-empirical potential suitable for molecular dynamics simulation of vitrification in Cu-Zr alloys. *J. Chem. Phys.* **151**, 214502 (2019).
38. B. Sadigh *et al.*, Scalable parallel Monte Carlo algorithm for atomistic simulations of precipitation in alloys. *Phys. Rev. B* **85**, 184203 (2012).
39. E. Maras, O. Trushin, A. Stukowski, T. Ala-Nissila, H. Jonsson, Global transition path search for dislocation formation in Ge on Si (001). *Comp. Phys. Commun.* **205**, 13 (2016).
40. N. Mattern *et al.*, Short-range order of Cu–Zr metallic glasses. *J. Alloys Comp.* **485**, 163 (2009).
41. N. Mattern *et al.*, Structural evolution of Cu–Zr metallic glasses under tension. *Acta Mater.* **57**, 4133 (2009).
42. G. J. Fan *et al.*, Thermophysical and elastic properties of Cu50Zr50 and (Cu50Zr50)95Al5 bulk-metallic-glass-forming alloys. *Appl. Phys. Lett.* **89**, 241917 (2006).
43. D. Wei *et al.*, Revisiting the structure–property relationship of metallic glasses: Common spatial correlation revealed as a hidden rule. *Phys. Rev. B* **99**, 014115 (2019).
44. F. Zhu, S. Song, K. M. Reddy, A. Hirata, M. Chen, Spatial heterogeneity as the structure feature for structure–property relationship of metallic glasses. *Nat. Commun.* **9**, 3965 (2018).
45. J. Ding, S. Patinet, M. L. Falk, Y. Cheng, E. Ma, Soft spots and their structural signature in a metallic glass. *Proc. Natl. Acad. Sci. U.S.A.* **111**, 14052 (2014).
46. T. Yanagishima, J. Russo, R. P. A. Dullens, H. Tanaka, Towards glasses with permanent stability. *Phys. Rev. Lett.* **127**, 215501 (2021).
47. C. Maloney, A. Lemaître, Universal breakdown of elasticity at the onset of material failure. *Phys. Rev. Lett.* **93**, 195501 (2004).
48. W. Jin, A. Datye, U. D. Schwarz, M. D. Shattuck, C. S. O'Hern, Using delaunay triangularization to characterize non-affine displacement fields during athermal, quasistatic deformation of amorphous solids. *Soft Matter* **17**, 8612 (2021).
49. H. J. Barlow, J. O. Cochran, S. M. Fielding, Ductile and brittle yielding in thermal and athermal amorphous materials. *Phys. Rev. Lett.* **125**, 168003 (2020).
50. A. S. Argon, L. T. Shi, Development of visco-plastic deformation in metallic glasses. *Acta Metall.* **31**, 499 (1983).
51. F. Ritort, P. Sollich, Glassy dynamics of kinetically constrained models. *Adv. Phys.* **52**, 219 (2003).
52. Z. Fan, E. Ma, Predicting orientation-dependent plastic susceptibility from static structure in amorphous solids via deep learning. *Nat. Commun.* **12**, 1506 (2021).
53. S. Plimpton, Fast parallel algorithms for short-range molecular dynamics. *J. Comput. Phys.* **117**, 1–19 (1995).
54. S. Nosé, A unified formulation of the constant temperature molecular dynamics methods. *J. Chem. Phys.* **81**, 511 (1984).
55. W. G. Hoover, Canonical dynamics: Equilibrium phase-space distributions. *Phys. Rev. A* **31**, 1695 (1985).
56. W. G. Hoover, Constant-pressure equations of motion. *Phys. Rev. A* **34**, 2499 (1986).
57. R. Malek, N. Mousseau, Dynamics of lennard-jones clusters: A characterization of the activation-relaxation technique. *Phys. Rev. E* **62**, 7723 (2000).
58. D. Rodney, C. Schuh, Distribution of thermally activated plastic events in a flowing glass. *Phys. Rev. Lett.* **102**, 235503 (2009).
59. E. Cances, F. Legoll, M.-C. Marinica, K. Minoukadeh, F. Willaime, Some improvements of the activation-relaxation technique method for finding transition pathways on potential energy surfaces. *J. Chem. Phys.* **130**, 114711 (2009).